JOURNAL OF SOLID STATE CHEMISTRY **141,** 105–113 (1998)
ARTICLE NO. SC987924

Cation Distribution in a Titanium Ferrite $Fe_{2.75}Ti_{0.25}O_4$ Measured by *in-Situ* Anomalous Powder Diffraction Using Rietveld Refinement

F. Bernard,*,[1] J. Lorimier,* V. Nivoix,* N. Millot,* P. Perriat,* B. Gillot,* J. F. Berar,† and J. C. Niepce*

*Laboratoire de Recherches sur la Réactivité des Solides, UMR 5613 CNRS, Université de Bourgogne, BP400, F-21011 Dijon, France; and †Laboratoire de Cristallographie, UPR 5031 CNRS, BP 166, F-38042 Grenoble Cedex 09, France

Received December 15, 1997; in revised form June 8, 1998; accepted June 9, 1998

Many ferrites contain different cations with various valence states and location in the spinel structure. In compounds such as these, only a combination of different techniques such as Mössbauer spectroscopy, IR analysis, and thermogravimetry allows the distribution of cations to be obtained. For very complicated distributions, the mathematical decomposition of derivative thermogravimetric curves (DTG) leading to quantitative distribution is uncertain. In this paper, we present an alternative technique based on resonant diffraction. The anomalous scattering of each cation in the crystalline material is used to determine its amount and position by Rietveld refinement. Since the energy for such an anomalous phenomenon is different for each cation, this technique should lead to the cation distribution whatever its complexity. Such a method in which the wavelength has to be varied with a great accuracy requires a synchrotron radiation source. The method has been tested in the simple case of titanium ferrites where the valence and location of the Fe cations can be adjusted through appropriate thermal treatments in reducing or oxidizing conditions. The aim of this paper is to validate this new method by comparing the cation distribution so obtained with that deduced from thermogravimetry experiments. In particular, we focus on its ability to distinguish between the different degrees of oxidation of the iron cations. Three different diffraction patterns have been recorded using the high-resolution goniometer on the BM02 Beam line at ESRF at the following energies: 7.105 keV, below the adsorption edges of both Fe^{2+} and Fe^{3+} cations; 7.120 keV, above the absorption edge for Fe^{2+} cations but below the Fe^{3+} edge and 7.135 keV, above the absorption edges of the Fe^{2+} and Fe^{3+} cations. © 1998 Academic Press

Key Words: **anomalous powder diffraction; *in-situ*; nanometric ferrite; Rietveld refinement; oxido-reduction treatment.**

1. INTRODUCTION

The magnetic and electrical properties of mixed oxides having the spinel structure strongly depend on the cation distribution. For example, concerning magneto-optic memories, for which these materials are good candidates, the presence of divalent cations such as Fe^{2+} or Co^{2+} in the octahedral sites increases the value of the coercivity significantly (1–5). For spinels prepared at low temperature, Gillot (6) has developed a quantitative method of analysis by derivative thermogravimetry (DTG). The cation distribution can be estimated directly, that is, both the valence and the location on tetrahedral (*A*) or octahedral (*B*) sites for each cation. This method is based on the fact that each cation oxidizes at a specific temperature characteristic of its location in the spinel lattice and of its degree of oxidation. Indeed, when the Fe-based spinel oxides contain more than one oxidizable cation, it has been demonstrated that each cation oxidizes in a well-defined temperature range closely related to the corresponding cation–oxygen distance. For example, the *B*-site Fe^{2+} ions are more mobile than the *A*-site Fe^{2+} ions, so that they are oxidized near 200°C whereas the *A*-sites are oxidized above 400°C. Such a difference in reactivity is due to the more covalent character of the tetrahedral Fe–O bond (7). In the more complicated case of ferrites containing different cations with various valence states that are located on the different sites in the spinel structure, the cation distribution can only be determined using mathematical decomposition of derivative thermogravimetric (DTG) measurements (8–9). Even though accurate knowledge of the initial and the final states of the cation distribution can be obtained, this method does not give any information about the real evolution of the cation distribution during oxidation and consequently does not allow the best distribution to be chosen in regard to the application. In addition, this method is not capable of distinguishing between cations with similar oxidation temperatures.

Rietveld refinements using *in situ* resonant X-ray diffraction data enable the distribution of the absorbing element over crystallographically distinct sites within a structure to be determined precisely, even when other elements with very similar atomic numbers are present (10). The intense white

[1] To whom correspondence should be addressed. E-mail: fbernard@satie.u-bourgogne.fr

0022-4596/98 $25.00

X-ray beams produced by synchrotron radiation are used in anomalous scattering powder diffraction experiments. These studies are typically performed close to elemental absorption edges and so are called "resonant" X-ray diffraction experiments. The edge position tends to vary with the electronic state of the resonant element and increases by several electronvolts for each unit increase in oxidation number, and so discernible differences between the atom scattering factors for different electronic states may be found from resonant X-ray diffraction experiments. Moreover, the edge shape provides information about the atom coordination, whereas the edge position provides information about the atom valences. Specific considerations for resonant studies are the wavelength and sample absorption. The energy spread and mean wavelength must be known accurately. Thus it is important to be able to select the wavelength accurately and to vary it in relation to the absorption edge position. Since the wavelength must be adjusted, synchrotron radiation should be used. The ESRF bending magnet beamline allows access to most of the elements through their K or L absorption edges.

From laboratory DTG experiments, it has been shown that the oxidation temperature of a cation depends on its mobility. In this paper, we report results obtained in the case of $Fe_{3-x}Ti_xO_4$. This system was chosen for its simplicity, since only the Fe cation can be found with various valences, the titanium being fixed with a degree of oxidation of 4 and only located in the octahedral sites. Different samples with various Fe^{2+}/Fe^{3+} ratios have been prepared and carefully characterized using both thermogravimetric analysis and X-ray diffraction. Consequently, a full crystalline structure description of the material at each oxidation step should be obtained. A structural refinement was also achieved using the Rietveld method, taking into account the anomalous effect in order to distinguish the different oxidation states of the iron cations.

2. THEORETICAL CONSIDERATIONS

2.1. Anomalous Scattering and X-Ray Absorption

In the past decade, the development and application of powder diffraction techniques at synchrotron sources have seen rapid progress (11). An important part is associated with the high resolution achieved. The use of the anomalous dispersion offers new opportunities: on the D2AM-CRG beamline, located at a bending magnet port of the ESRF, energies between 5 and 25 keV can be used. In the past, the only application of anomalous scattering was to provide a contrast between neighboring elements. However, a recent application of anomalous scattering to powder diffraction is the site-selective spectroscopic study of samples in which the same element can be present in different oxidation states (12). The chemical shift of the adsorption edge between oxidation states is very small, typically a few electronvolts,

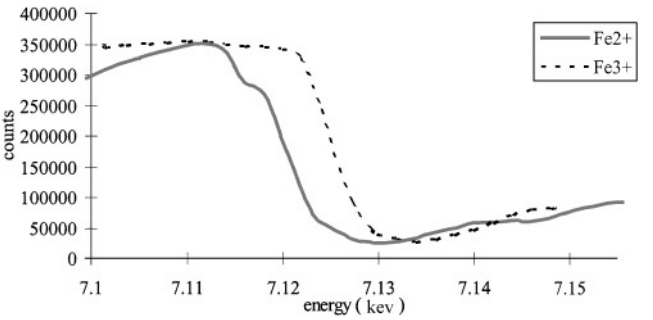

FIG. 1. Absorption edge curves obtained from FeO (only Fe^{2+} cations) and Fe_2O_3 (only Fe^{3+} cations) powders analyzed in transmission.

and if the EXAFS oscillations strongly depend on the neighboring of the selected atom, the edge position is quite stable for various oxidation states. This shift can then be used to characterize the occupancy of sites by the various valency states of an element.

The effective values of the anomalous dispersion term strongly depend on the resolution achieved by the experimental setting. The absorption edges of the simple oxides FeO (only Fe^{2+}) and Fe_2O_3 (only Fe^{3+}) have been recorded on a diffractometer. These oxides well reproduce the oxidation states but induce some small deviation at high energy, as the EXAFS oscillations are not identical to those in our sample. As an example, these absorptions are represented in Fig. 1; the shift between Fe^{2+} and Fe^{3+} appears to be only 6 eV.

2.2. Atomic Scattering Factor Refinement

The "usual" procedure has been followed to obtain the effective value of anomalous terms in the structure factor. The atomic scattering factor for X-rays, F, contains the normal term, f_0 and an anomalous dispersion contribution consisting of real, f', and imaginary, f'', terms depending on the energy (E):

$$F = f_0(s) + f'(E) + if''(E). \quad [1]$$

f'' has been calculated from the observed absorption $\mu(E)$, according to the formula

$$f''(E) = \frac{mc}{2he^2N} E\mu(E), \quad [2]$$

where m is the electron mass, c the light velocity, h Planck's constant, e the electron charge, and N the density number of atoms.

When f'' is known, f' can be calculated by the Kramers–Kronig relation:

$$f'(E) = (2/\pi)\int_0^\infty \frac{E^* f''(E^*)}{(E^2 - E^{*2})} dE^*. \quad [3]$$

By the method described by Bernard *et al.* (13), the calculated values of $f'(E)$ and $f''(E)$ for each cation on Ti ferrite have been determined. From these values the diffraction data have been recorded at three energies: the first at 25 eV below the edge, the second at the maximum f' relative of the Fe^{2+} curve, and the last 15 eV higher. Consequently, the following relation describes the structure factor:

$$F = \sum_j (f_j + f'_j + if''_j)\cos 2\pi(hx_j + ky_j + lz_j) + i\sum_j (f_j + f'_j + if''_j)\sin 2\pi(hx_j + ky_j + lz_j). \quad [4]$$

In powder diffraction, Friedel pairs of reflections (h, k, l) and $(-h, -k, -l)$ are always recorded simultaneously. F^+ and F^- are their respective structure factors with only one anomalously scattering element in the unit cell:

$$F^{\pm} = [A + a(f' + if'')] \pm i[B + b(f' + if'')], \quad [5]$$

where A (B) and a (b) are the summed cos (sin) terms for the normal and anomalous contributions, respectively. Moreover, in the case of a powder having a symmetric center located at the origin of the lattice, the expression of the apparent intensity can be reduced to the following equation:

$$I = k[(A + af')^2 + af''^2]. \quad [6]$$

For different wavelengths close to an edge, a variation of the peak relative intensity can be observed. This difference will be used to determine the cation distribution using Rietveld refinement (14).

3. EXPERIMENTAL DETAILS

3.1. Crystallographic Considerations

Ferrite samples with spinel structure AB_2O_4 have a face-centered cubic crystalline lattice and space group $Fd3m$ (JCPDS No 19–629). The oxygen ions occupy 32 positions and are arranged in a cubic close packed structure. Such an arrangement of ions leaves 64 tetrahedral and 32 octahedral holes as possible sites for cations. Of these sites only 8 tetrahedral and 16 octahedral sites are occupied. In reference to Barth and Posnjak (15), the studied Ti ferrite, $Fe^{2+}_{1.25}Fe^{3+}_{1.5}Ti^{4+}_{0.25}O^{2-}_4$, has an "inverse" spinel structure with similar cations occupying different coordinating positions. During the oxidation process at low temperature, this structure tends toward the maghemite structure, though this depends on the grain size, the grain shape, and thermal treatment of the sample, which can modify the order between the lattice vacancies created during oxidation.

3.2. Synthesis Conditions of Samples

In reference to Neel (16), a nanometric Ti ferrite can be written as $Fe^{2+}_{1.25}\ Fe^{3+}_{1.5}\ Ti^{4+}_{0.25}\ O^{2-}_4$. It has been synthesized using a soft-chemistry route, which is a well-known method for obtaining nanometric powder. In nanometric compounds, the cations in the spinel structure can oxidize at low temperatures without any phase transformation, leading to a cation-deficient spinel with formula $Fe_{2.75}Ti_{0.25}O_{4+\delta}$, where δ is the deviation from stoichiometry (or the number of fixed oxygen atoms). This modification is due to a change in the anion–cation ratio, consecutive to formation of vacancies. Indeed, in a previous study on the influence of crystallite size on the oxidation mechanism of annealed magnetite (17), it has been shown that for crystallite sizes below about 300 nm, cation-deficient γFe_2O_3 spinel can be obtained between 150 and 350°C. During the oxidation process, there is a δ gradient, which is higher near the surface than in the bulk. At the end of the oxidation of the Fe^{2+} cation, the deviation from the stoichiometry is homogeneous inside the whole particle and equal to the maximum value, corresponding to γFe_2O_3. This phenomenon is different from that observed for larger particles sizes, where the formation of αFe_2O_3 is explained according to the sequence of reactions

$$\begin{aligned} Fe_3O_4 &\rightarrow Fe_3O_{4+\delta}(\text{surface}) + Fe_3O_4(\text{core}) \\ &\rightarrow \alpha Fe_2O_3(\text{surface}) + Fe_3O_4(\text{core}) \\ &\rightarrow \alpha Fe_2O_3(T > 500^\circ\text{C}) \end{aligned}$$

The general procedure of soft chemistry is as follows: (1) suitable amounts of ferrous, ferric, and titanium chloride in a HCl solution are dissolved (2). An ammonia solution is added, which leads to instantaneous precipitation of Ti ferrites according to the following equation:

$$(1 + x)Fe^{2+} + (2 - 2x)Fe^{3+} + xTi^{4+} + 8OH^- \rightarrow Fe_{3-x}Ti_xO_4 + 4H_2O$$

During this reaction, the system is continuously stirred and particles are then separated by centrifugation. (3) After four washings with deionized water under ultrasonication for 5 min followed by centrifugation at 3500 rpm for 5 min, a sol is obtained. (4) Freeze drying of the sol leads to a dry spinel precipitate evidenced from XRD experiments. (5) Calcination in air at 400°C for 10 h and heating at 600°C 1 h is carried out to eliminate remaining impurities while limiting crystalline growth. (6) Thermal treatment under reducing conditions at 500°C with $H_2/N_2/H_2O$ gas mixtures is performed to obtain stoichiometric ferrite $Fe_{3-x}Ti_xO_{4+\delta}$ with $\delta = 0$.

The relative concentrations of different gases to reach stoichiometry were determined by studying the relationship

at 500°C between the deviation from stoichiometry δ (as a function of the oxygen partial pressure pO_2) given by the gas mixture and measured by an EMF cell and the deviation from the stoichiometry deduced from the mass variation measured by TGA. The stoichiometry $\delta = 0$ is obtained at a particular temperature in the range of oxygen partial pressure where δ does not vary with pO_2.

The device used, which has been developed by Aymes *et al.* (18), allows the control of the oxygen partial pressure using the chemical equilibrium between H_2, O_2, and H_2O. This apparatus was used to synthesize four samples with different δ. The first one (P1) corresponds to a stoichiometric state ($\delta = 0$). It was reduced 1 h at 500°C under $H_2/N_2/H_2O$ gas mixtures that give a pO_2 of 1.4×10^{-29} atm. Because of the great reactivity of this sample toward oxygen, this step was done *in situ* in the thermobalance and in the X-ray reaction chamber. The other samples (P2, P3, and P4) were obtained by annealing in oxidizing conditions, consisting of linear heating under N_2/O_2 gas mixtures (80%/20%) up to 100°C (P2), 150°C (P3), and 350°C (P4). An annealing under nitrogen at higher temperature follows each oxidation (50°C higher) in order to homogenize δ inside the whole particle. The deviation from stoichiometry was determined using a Setaram TAG24 thermobalance as reported in Ref. 18.

3.2.1. TGA experiments. Each powder sample, i.e., reduced powder (P1), partially oxidized powder at 100°C (P2), and partially oxidized powder at 150°C (P3), and fully oxidized powder at 350°C (P4), was studied by thermogravimetry analysis. These powders were totally oxidized to obtain the δ value from the value of the mass gain. The results concerning the oxidation states for a titanium ferrite are summarized in Table 1. This table shows the evolution of $\Delta m/m$, the Fe^{2+}/Fe^{3+} ratio, and δ determined from TGA curves for the various oxido-reduction treatments. It shows that the Fe^{2+}/Fe^{3+} ratio decreases as the oxidation temperature increases.

3.2.2. In situ XRD experiments. The different samples were investigated using data collected with an Inel CPS120 diffractometer and Co$K\alpha_1$ radiation ($\lambda = 0.178897$ nm). The diffraction pattern was scanned over the 2θ range 20–130° with a step length of 0.03° (2θ) and a counting time of 3600 s by step. Laboratory studies have shown that the sample is slowly oxidized at room temperature in air; therefore diffraction experiments were carried out with the XRK900 reaction chamber (Anton Parr) and strictly controlled $H_2/N_2/H_2O$, N_2, or $N_2 + O_2$ gas flows. With this X-ray chamber, *in situ* XRD experiments were performed in the same oxido-reduction treatments as those carried out in the thermobalance in order to characterize the lattice parameter (least-squares method) and the crystallite size, which is determined by the Halder–Wagner method (19). The results obtained are summarized in Table 2.

The lattice parameter decreases with the overall oxidation and appears to be reproducible during oxidation–reduction cycles. The creation of vacancies and the decreasing number of Fe^{2+} cations which have an ionic radius greater than Fe^{3+} cations induce a lattice shrinking. At the same time, the grain size increases slightly with the oxidation temperature but remains small. This increase is due to the formation of additional crystalline cells associated with the oxygen fixation.

3.3. Resonant Diffraction Experiments

Anomalous scattering experiments were performed on the D2AM-CRG beamline at ESRF using the X-ray chamber XRK900. Three different diffraction patterns were recorded using a high-resolution goniometer: one, at 7.105 keV ($\lambda_1 = 0.1745$ nm), below the absorption edges, one at 7.120 keV ($\lambda_2 = 0.1741$ nm), for which only Fe^{2+} cations contribute to the anomalous effect, and one at 7.135 keV ($\lambda_3 = 0.1738$ nm), for which both the Fe^{2+} and Fe^{3+} cations contribute to the anomalous effect. For each state, three data sets were collected on the seven-circle diffractometer equipped with a Si(111) analyser. To optimize the use of the beam, the full pattern was not recorded. The selected diffraction lines were chosen, remembering that the *B* (octahedral) or the *A* (tetrahedral) sites do not contribute to all lines according to their *h*, *k*, *l* values. The reflection conditions for the tetrahedral sites are $h = 2n + 1$ or $h + k + l = 4n$, and for the octahedral sites $h = 2n + 1$ or $h,k,l = 4n + 2$ or

TABLE 1

Evolution of $\Delta m/m$, δ (Stoichiometry Deviation), and Fe^{2+}/Fe^{3+} Ratios, Determined by ATG Experiments versus Different Oxidation States Applied on Powders P1, P2, P3, and P4

Sample	$\Delta m/m$ (%)	δ	Fe^{2+}/Fe^{3+}
P1	3.67	0.098	0.61
P2	2.51	0.265	0.36
P3	1.66	0.396	0.2
P4	0	0.6251	0

TABLE 2

Evolution of the Cell Parameter and the Crystallite Size, Determined at Room Temperature in Nitrogen, Gas Flow, after Each Oxido-Reduction Treatment

Sample	a (nm)	Particle size (nm)
P1	0.84055	42
P2	0.83934	47
P3	0.83792	49
P4	0.83442	51

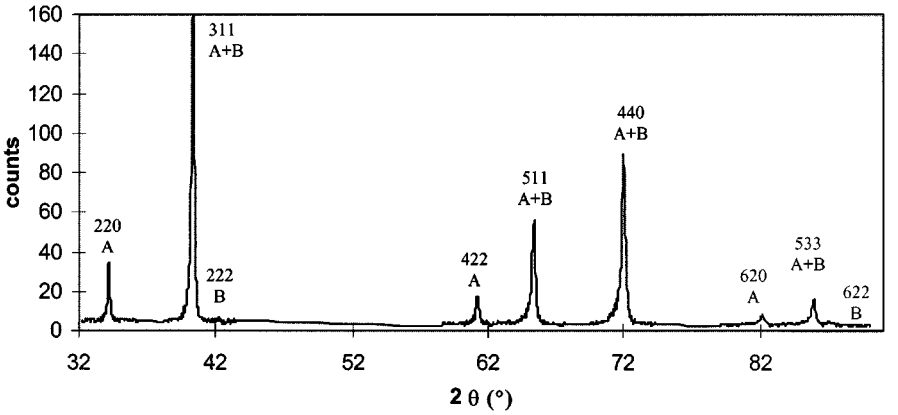

FIG. 2. Example of data set with the *B*-site (octahedral) sensitive lines and the *A*-site (tetrahedral) sensitive lines.

$h,k,l = 4n$. An example of the observed data is given in Fig. 2.

Data sets were recorded for the reduced and three oxidized states (100, 150, and 350°C) of the titanium ferrite. However, a technical cooling problem occurred which had modified the monochromator tuning, and data obtained for the partially oxidized sample at 100°C (P2) were not reliable. For each state, the data sets were processed by the Rietveld method using the XND1.10 program (20), which allows all data sets to be refined simultaneously. To provide more data, a whole pattern recorded in the laboratory was added to the refinement. The quality of the fit can be followed with respect to different control parameters such as Gof (goodness of fit, whose limit tends to 1) and R_{wp} (reliability factor: weighted gap between measured and calculated values; it must be close to or less than 10%). This software allows the structure factors (real part represented by $A + af'$ and imaginary part represented by af'') of each reflection to be displayed, as shown in Table 3.

TABLE 3
Variation of the Imaginary (af'') and Real Parts ($A + af'$) of the Structure Factors for Sample P1 at Different Wavelengths near the Fe *K*-edge

	Structure factor					
	$\lambda_1 = 1.745$ Å		$\lambda_2 = 1.741$ Å		$\lambda_3 = 1.783$ Å	
hkl	$A + af'$	af''	$A + af'$	af''	$A + af'$	af''
220	− 470	− 15	− 396	− 15	− 653	0
311	− 674	− 21	− 573	− 44	− 905	− 26
222	68	22	− 30	68	271	52
422	335	14	263	14	511	0
511	586	20	488	43	808	25
333	412	20	314	43	634	25
440	1296	35	1071	79	1603	49

Table 3 shows that the structure factors are strongly dependent on the energy. For example, in the case of the line (222), the real part value of structure factor varies with the wavelength (68 at 0.1745 nm, − 30 at 0.1741 nm, and 271 at 0.1738 nm). Nevertheless, these structure factor differences are not easily discerned from the relative peak intensities at each energy as can be seen in Fig. 3a, corresponding to the raw data. However, as shown in Fig. 3c, corresponding to the raw data after background and scale factor corrections, the relative intensity difference for the three wavelengths previously determined seems more evident.

4. RESULTS AND DISCUSSION

From X-ray diffraction patterns, several refinements were performed according to the following steps: First, the fully oxidized (P4) refinement was carried out to determine the Fe/Ti ratio (all Fe^{2+} cations have been oxidized to Fe^{3+} cations) and the number of vacancies. For the P4 sample, the space group is $P4_132$. Thus, the 16 octahedral sites in the lattice are decomposed in 12 + 4 sites respectively called B_1 and B_2. Second, the partially oxidized (P3) and reduced (P1) sample refinements, using the Ti value which was determined previously, enabled us to obtain the amount and the location of Fe^{2+} and Fe^{3+} cations inside the spinel structure.

Figure 4 represents for powder P3 as an example the experimental and calculated diffraction patterns and the difference in the angular domain 55–75° recorded at the λ_1, λ_2, and λ_3 wavelengths previously determined.

This figure shows a good agreement between them. The results of refinements carried out on these powders are listed in Table 4. The cation distribution and the quality of the Rietveld refinement throughout the Gof and R_{wp} are presented. To ensure they are consistent, other cation distributions were tested and in all cases the overall quality of

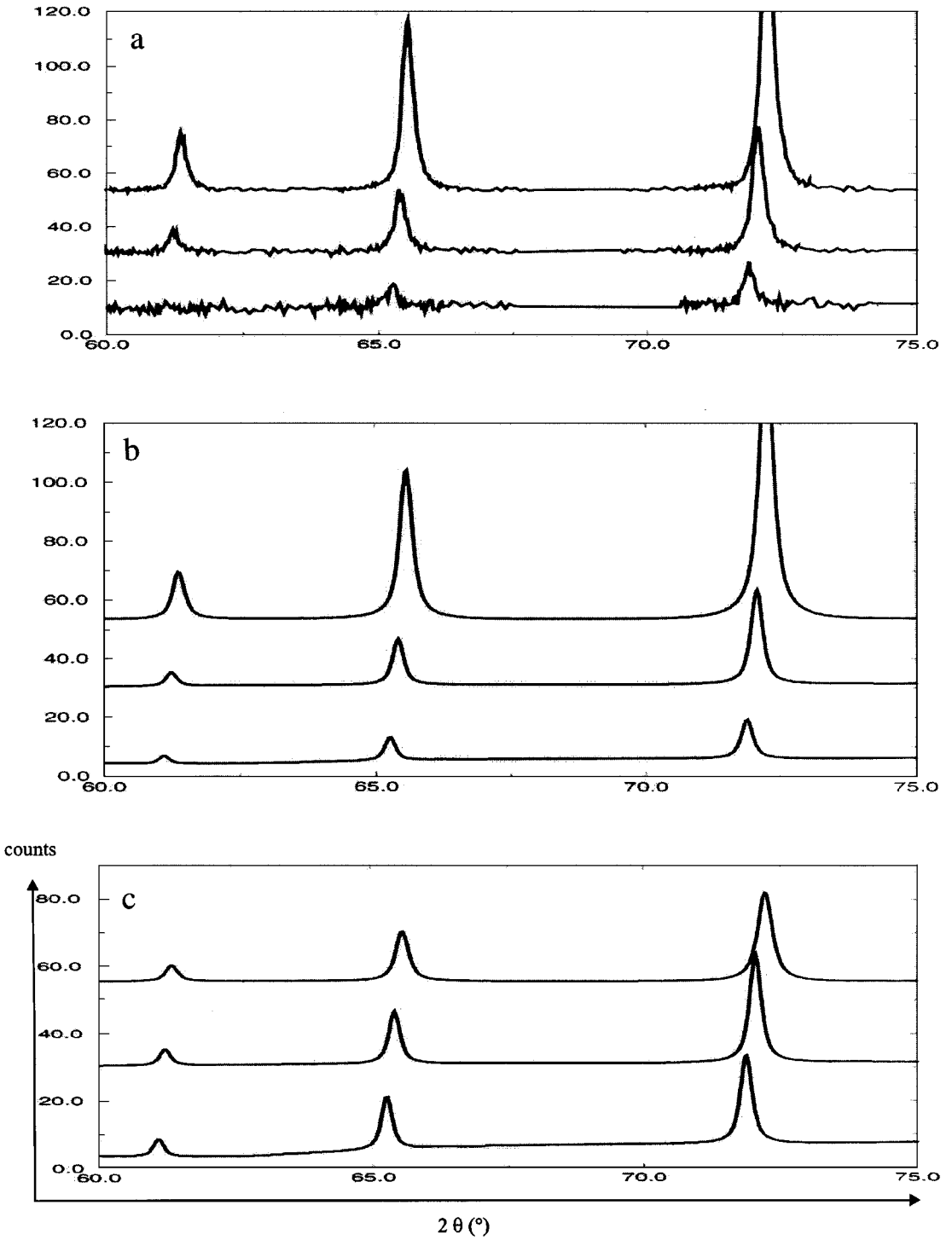

FIG. 3. Variation of the peak intensities for sample P1 versus the wavelengths and the nature of the correction applied: (a) raw data, (b) raw data after background correction; (c) raw data after background and scale factor corrections.

refinement decreased. The quite high error on the cation amounts is due to the poor quality of some X-ray patterns, in particular those recorded at 7.135 keV.

This analysis gives the amount and the location of the Fe^{2+}, Fe^{3+}, and Ti^{4+} cations in the spinel structure. The values obtained are in agreement with the chemical knowledge of the ferrite. The Rietveld refinement shows that Fe^{2+} cations are only located on octahedral sites. This observation is in perfect agreement with the DTG experiment. For example, Fig 5, showing the DTG of sample P1, presents

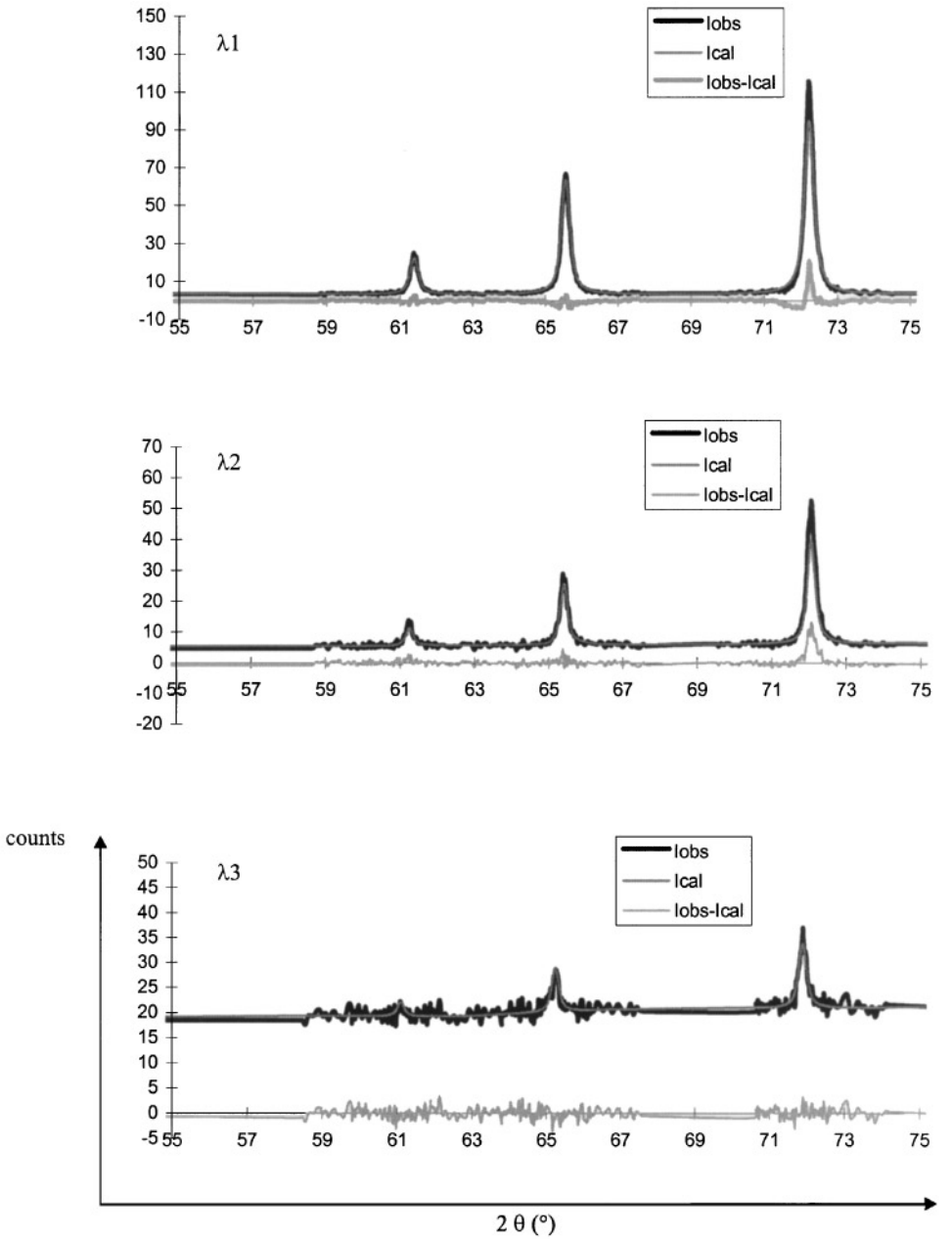

FIG. 4. Refinements and diffraction patterns obtained for sample P3 at three wavelengths ($\lambda_1 = 0.174495$ nm, $\lambda_2 = 0.174122$ nm, and $\lambda_3 = 0.17378$ nm), where I_{obs} is the observed intensity, I_{cal} the calculated intensity after refinement, and $I_{obs} - I_{cal}$ the difference.

only one oxidation peak at 200°C, which is characteristic of the presence of Fe^{2+} cations in octahedral sites.

In addition, it appears that the Ti^{4+} cations are exclusively located on octahedral sites and that they prefer to occupy the B_1 sites in the case of the fully oxidized material. This analysis also gives the number and location of the vacancies. Oxidation leads to the appearance of vacancies, which prefer to occupy an octahedral site. This observation is in agreement with earlier neutron experiments (21).

Table 5 compares DTG with the anomalous diffraction results. It is obvious that the Fe^{2+}/Fe^{3+} ratio decreases as oxidation temperature increases. For the reduced sample this ratio is equal to 0.65 whereas a value of 0.185 is obtained for the partly oxidized state and a value of 0 is obtained for the fully oxidized sample. At the same time, the number of vacancies increases. The values obtained from Rietveld refinement using this technique are in good agreement with thermogravimetric experiments, allowing the

TABLE 4

Evolution of the Amount and the Location of Fe^{2+}, Fe^{3+}, and Ti^{4+} Cations and Vacancies (Represented by □) in the Different Sites (*A* Tetrahedral, *B*, B_1, B_2 Octahedral) of the Spinel Structure for the Different Oxidation States Represented by P_1, P_3, and P_4[a]

	P1	P3	P4
$Fe^{3+}_{tetrahedral}$	0.97 ± 0.02	0.99 ± 0.01	0.95 ± 0.02
$□_{tetrahedral}$	0.03 ± 0.02	0.01 ± 0.01	0.05 ± 0.02
$Fe^{2+}_{octahedral}$	1.08 ± 0.07	0.40 ± 0.05	0
$Fe^{3+}_{octahedral}$	0.65 ± 0.07	1.19 ± 0.05	B1: 0.97 ± 0.03 B2: 0.46 ± 0.03
$Ti^{4+}_{octahedral}$	0.25	0.23	B1: 0.19 ± 0.03 B2: 0.03 ± 0.03
$□_{octahedral}$	0.02 ± 0.07	0.18 ± 0.05	B1: 0.34 ± 0.03 B2: 0.01 ± 0.03
O^{2-}	4	4	4
λ_1 R_{wp}	12%	11%	10%
λ_2 R_{wp}	12%	12%	6%
λ_3 R_{wp}	10%	6%	6%
Overall R_{wp}	12%	10%	6%
Overall Gof	1.32	1.61	5.52

[a]The quality of the Rietveld refinements is indicated by the overall Gof (goodness of fit), the overall R_{wp} (reliability factor), and the R_{wp} obtained for each wavelength (λ_1, λ_2, λ_3).

Fe^{2+}/Fe^{3+} ratio to be known (Table 5). The good agreement between the two sets of results indicates that this method can be used for the *in situ* characterization of the cation distribution of Ti ferrites with different Fe^{2+}/Fe^{3+} ratios obtained from different oxido-reduction annealings. These results allow one to use the anomalous diffraction experiment to determine the cation distribution in more complicated cases where DTG cannot be used when there are two or three cations that can be oxidized at nearby temperature.

Nevertheless, concerning the study of the P1 sample (stoichiometric compound), a careful analysis of the data set obtained in the reduced state puts in evidence some asymmetry around the low angles. Since such an asymmetry disappears when the Fe cations are oxidized, it cannot be attributed to an instrumental aberration and must be due to a gradient of the Fe^{2+}/Fe^{3+} ratio from the surface to the bulk in each nanoparticle. Due to the slow cooling to room temperature after the appropriate annealing at 500°C leading to stoichiometry, some hydrogen has to be introduced into the furnace to avoid oxidizing some Fe cations. This leads to a correlative reduction of the Fe cations located on the surface, so that the Fe^{2+}/Fe^{3+} ratio is effectively larger at a distance of approximately 2 nm from the surface despite a choice of relatively large grains (40 nm). Consequently, to perform the structural refinement of this state, a simple model with two phases has been used; one of these phases corresponds to the fully reduced state.

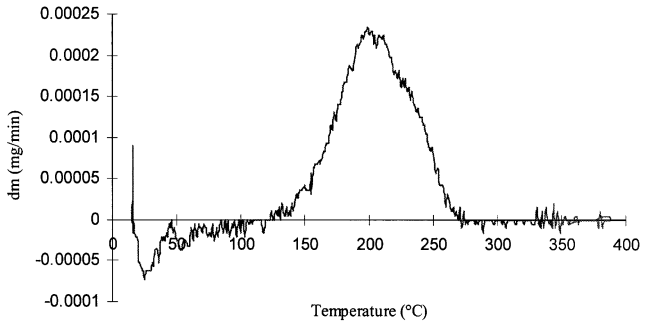

FIG. 5. DTG curve of sample P1 obtained on the Setaram TAG24 thermobalance. Only one oxidation peak is observed (at 200°C), which is characteristic of the oxidation of Fe^{2+} cations located at octahedral sites.

TABLE 5

Comparison of the Fe^{2+}/Fe^{3+} Ratio and Cell Parameter Obtained Using TGA and XRD Experiments and by Resonant Diffraction Experiments Using Rietveld Refinement

	Fe^{2+}/Fe^{3+} ratio		*a* (nm)	
Sample	DTG	Resonant XRD	CPS 120 Dijon	D2AM
reduced	0.61	0.65	0.84055	0.84000
oxidized at 150°C	0.20	0.185	0.83792	0.83754
fully oxidized	0	0	0.83442	0.83442

Since the aim of this work was to obtain the cation distribution in order to control magnetic properties, coercivity was also studied with a SQUID. The coercivity was measured from room temperature to 5 K for these different powders. Figure 6 shows that the coercivity at 5 K is maximal when the Fe^{2+}/Fe^{3+} ratio is greater.

5. CONCLUSION

These results obtained with the titanium ferrite varying the Fe^{2+}/Fe^{3+} ratio show that it is possible to use anomalous powder diffraction to reach with a good accuracy the cation ordering in such compounds. A Rietveld refinement using the anomalous scattering of the atom species of the crystalline material is able to give information about the amount and position of this atom in the crystalline structure. Consequently, we have given a full crystalline structure description of this nanometric ferrite after different oxido-reduction treatments using the Rietveld method. The structural refinement allowed us to establish the location of the various cations on both the octahedral and the tetrahedral sites and of the resulting vacancies. Nevertheless, from a methodological point of view, two principal improvements would need to be performed to have a better refinement accuracy. First, due to a large fluorescence above the

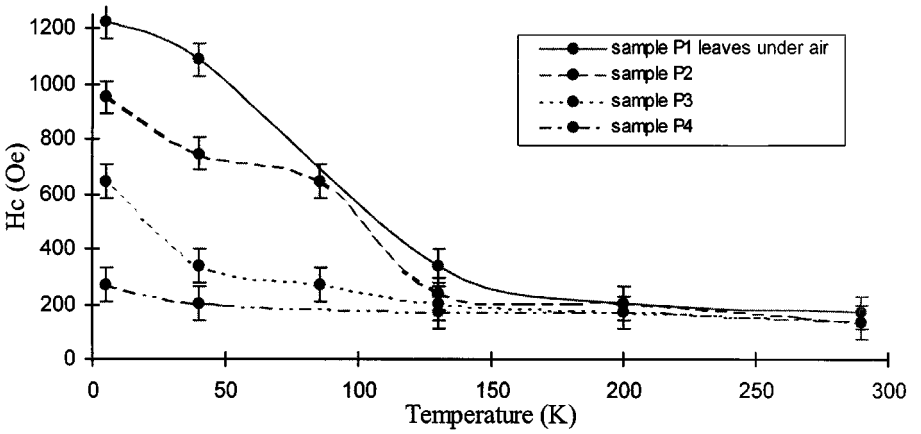

FIG. 6. Evolution of the coercivity versus the temperature (from 5 K to room temperature) for different samples containing various Fe^{2+}/Fe^{3+} ratios.

Fe edge, it is essential to increase the recording time for each data set to have a sufficient statistical level to carry out Rietveld refinement in the usual conditions. Second, it seems useful to record data at more than three energies to ensure significance of the anomalous effect to distinguish the different oxidation states of the iron cations and to determine the anomalous factors with more accuracy. Moreover, to minimize the heterogeneity that appears during the cooling, the most useful experiments would be to record the X-ray diffraction patterns at high temperature under an appropriate reducing gas mixture for which the stoichiometric compound would be thermodynamically stable. Indeed, at high temperature (around 450°C), it would then be possible, in contrast to room temperature, to study perfectly homogeneous ferrites with a smaller size (20 nm) and two different Fe^{2+}/Fe^{3+} ratios, one corresponding to the stoichiometry under a reducing gas mixture, the other with all Fe cations fully oxidized to Fe^{3+} cations under an oxidizing gas mixture. In the future, this method may be extended to samples with numerous cations with various valencies, checking the edges of each cation.

ACKNOWLEDGMENTS

The authors thank the Laboratoire d'Optique et de Magnétisme de Versailles for the coercitive field measurement. They also thank all of the personnel of the Beamline BM02, but in particular E. Doorhyee of the Beamline BM16 at the ESRF.

REFERENCES

1. L. Bouet, P. Tailhades, and A. Rousset, *J. Magn. Magn. Mater.* **153,** 389 (1996).
2. M. C. Deng, and T. S. Chin, *J. Magn. Magn. Mater.* **120,** 37 (1993).
3. P. Tailhades, C. Sarda, P. Mollard, and A. Rousset, *J. Magn. Magn. Mater.* **104–107,** 369 (1992).
4. P. Tailhades, P. Mollard, A. Rousset, and M. Gougeon, *IEEE Trans. Magnet*, **6,** 1822 (1990).
5. A. Goldman, "Modern Ferrite Technology." Van Nostrand Reinhold, New York, 1990.
6. B. Gillot, *J. Solid State Chem.* **113,** 163 (1994).
7. J. B. Goodenough, and A. L. Loeb, *Phys. Rev.* **98,** 391 (1955).
8. B. Gillot, B. Domenichini, L. Bouet, P. Tailhades, and A. Rousset, *Solid State Ionics* **63–65,** 620 (1993).
9. B. Gillot, B. Domenichini, and P. Perriat, *Solid State Ionics*, **84,** 303 (1996).
10. J. P. Attfield, *J. Phys. Chem. Solids* **52,** 1243 (1991).
11. D. E. Cox and A. P. Wilkinson, "Resonant anomalous X-Ray scattering," Elsevier Science, pp. 195–219, 1994.
12. J. P. Attfield, *Nature* **343,** 46 (1990).
13. F. Bernard, J. Lorimier, V. Nivoix, N. Millot, J. C. Niepce, P. Perriat, B. Gillot, M. Ferlet, and J. F. Berar, *Mater. Sci. Forum* **278–281,** 594 (1998).
14. H. M. Rietveld, *J. Appl. Crystallogr.* **2,** 65 (1969).
15. T. F. Barth and E. Posnjak, *Z. Kristollogr.* **82,** 325 (1932).
16. L. Neel, *Adv. Phys.* **4,** 191 (1955).
17. B. Gillot, A. Rousset, and G. Dupre, *J. Solid State Chem.* **25,** 263 (1978).
18. D. Aymes, N. Millot, V. Nivoix, P. Perriat, and B. Gillot, *Solid State Ionics* **261,** 101 (1997).
19. N. C. Halder and C. N. J. Wagner, *Acta. Crystallogr.* **20,** 312 (1996).
20. J. F. Berar, IUG Sat. Meeting "Powder Diffraction," Toulouse, (1992).
21. G. Greaves, *J. Solid. State Chem.* **49,** 325 (1983).